Int. J. Electron. Commun. (AEÜ) 124 (2020) 153108

Contents lists available at ScienceDirect

International Journal of Electronics and Communications (AEÜ)

journal homepage: www.elsevier.com/locate/aeue

Regular paper

Indoor amplify-and-forward power-line and visible light communication channel model based on a semi-hidden Markov model

Oluwafemi Kolade [a,c], Ayokunle Damilola Familua [b], Ling Cheng [a,*]

[a] Optical Communication Laboratory, School of Electrical and Information Engineering, University of the Witwatersrand, Johannesburg, South Africa
[b] Center for Telecommunications, Department of Electrical and Electronic Engineering Science, University of Johannesburg, South Africa
[c] Sibanye-Stillwater Digital Mining Laboratory (DigiMine), Wits Mining Institute (WMI), University of the Witwatersrand, Johannesburg, South Africa

ARTICLE INFO

Article history:
Received 4 October 2019
Accepted 30 January 2020

Keywords:
Baum-Welch
Channel model
Fritchman
Hybrid channel
Markov model
Power-line
Software-defined radio
Visible light

ABSTRACT

In this paper, the channel model of a multicarrier, indoor amplify-and-forward (AF) hybrid power-line communication (PLC) and visible light communication (VLC) channel is demonstrated. Measurements are obtained from different positions between the VLC transmitter and receiver in an indoor testbed with the aid of software-defined radios. Using the obtained measurements, channel models are derived using a semi-hidden Markov model (SHMM) with the aid of a Fritchman channel state representation model. The Baum-Welch algorithm is then used to re-estimate and validate the derived models. Results presented show the error-free run distribution in the hybrid channel and the probability of error from the obtained measurements. The re-estimated probability of error ($\bar{P}_e$) of each measured indoor scenario is also seen to match the corresponding measured P_e, showing the validity of the derived SHMM models.

1. Introduction

Communication via visible light such as in light emitting diodes (LEDs) contributes to the promising alternatives to wireless and cable-based communication required for 5G and Internet of Things (IoT). Naturally, indoor illumination, vehicle lights and other outdoor illumination and signage prefer LEDs due to its long life and low power consumption. Hence, the ability of LEDs to deliver data communication using visible light communication (VLC) in areas where line of sight (LOS) communication is sufficient, provides alternative means of supporting the bandwidth requirements of 5G and IoT. Power-line communication on the other hand utilizes the electric wave such as in indoor power cables to convey higher frequency, data signals via the same power cable. Since LED luminaries are lit up by power cable installations, for example, in an indoor environment, LED luminaries can extend their link length to the network backbone or surrounding network architecture using the power-line.

Experimental and theoretical channel models of the memoryless power-line channel show that the power-line noise is not only Gaussian but consists of frequency disturbances, impulsive noise (IN) and signal attenuation with distance [1–4]. IN for example, is observed to occur over a period of time or in bursts, was estimated to persist for not longer than 0.1 ms [5] and could occur as a result of devices plugged into the channel. Impulses also occur as frequency disturbances, affecting a certain frequency over a period of time. Since the power-line channel exhibits a bus topology in which the different paths in the bus network all convey the signal, each path suffers a different attenuation corresponding to the length of the path [4]. As a result, integrating PLC with VLC using decode-and-forward (DF) [6–8] methods becomes attractive in order to improve the quality of the attenuated signal forwarded to the VLC transmitter module. Multi-carrier modulation schemes can further assist with improving the data rate of the hybrid PLC-VLC setup [9,10]. However, the performance of DF methods come with increased complexity and additional circuitry and wiring in areas where minimal changes may be required to the existing PLC-VLC integration. The alternative is to forward the PLC signal without demodulating [11–13] and a further amplification of the PLC signal in the amplify-and-forward (AF) ensures the VLC signal is enough to drive the LED. While AF is more error-prone, it becomes attractive in environments where minimal circuitry changes are required to the existing PLC-VLC circuitry. The theoretical channel model of VLC is assumed to be Gaussian and consists of shot noise and thermal noise [14] generated from the receiver

* Corresponding author.
E-mail address: ling.cheng@wits.ac.za (L. Cheng).

https://doi.org/10.1016/j.aeue.2020.153108
1434-8411/

circuitry. Therefore, an AF PLC-VLC setup suggests the noise in the PLC channel is also amplified at the VLC transmitter. For a memoryless, integrated PLC-VLC channel, a simple model which combines the PLC noise with the VLC noise is found in [15]. Furthermore, using the Welch method, a non-parametric approach is used in [16] to model the frequency response of the PLC channel using the number of taps, cable parameters and multi-path channel topology similar to [4].

Markov models [17–19] have been used as a convenient technique for modelling channels with memory in order to produce approximate statistical models of the respective channel. For example, Markov models in [20–22] are used to model the bursts in the PLC channel with a derived model that follows the Middleton Class A model found in [23]. A testbed in a controlled environment is the starting point to obtain measurements and the PLC testbed measurements in [24] confirm that noise in the PLC link occurs in bursts. Hence, the Fritchman three-state model in [24] proposes two states to characterize the good state while one state characterizes the events of the channel in an error state. As a result, a semi-hidden Markov model (SHMM) which uses the Fritchman model (FM) [25] is then used to develop an error distribution model of the PLC channel with memory. A similar modelling approach of channels with memory is applied to the VLC channel in [26] with the consideration of pulse width modulation interference. The equivalent DF statistical model using SHMM and FM was obtained in [27] using single carrier modulation which combines frequency shift keying (FSK) with On-Off keying (OOK). Furthermore, an AF hybrid PLC-VLC integration in [13] demonstrates the bit error rate for a multi-carrier modulation in the hybrid channel. However, a statistical model for the AF hybrid PLC-VLC channel with memory does not exist.

In this paper, the error distribution of the hybrid AF PLC-VLC is obtained using SHMM with the aid of a FM. The measurements are taken using a testbed setup in an indoor office environment. Multicarrier modulation using orthogonal frequency division multiplexing (OFDM) with binary phase shift keying (BPSK) is pre-processed on a computer using MATLAB. The data is then transmitted over a Universal Software Radio Peripheral (USRP) N210 transmitter (Tx). The PLC signal is forwarded to the VLC module, amplified enough to drive the LED and transmitted over the LED unit. The receiver photodiode (PD) converts the current from the changing intensity of the LED to a voltage using a trans-impedance amplifier (TIA). The received voltage samples are then converted by the USRP receiver (Rx) and post-processed on a computer to demodulate the samples. The error sequence is then used to derive the steady-state transition probabilities of the channel using the Baum-Welch algorithm [28]. These transition probabilities can then be used to re-generate an approximate, statistical error sequence using the error vector generation algorithm [29]. Error-free run (EFR) distribution plots show that the measured sequences and the re-generated sequences match in most regions and the derived probabilities can be used for channel analysis in terms of suitable parameters of modulation and error correction schemes which can mitigate the effect of the channel noise.

2. Channel modelling

Consider a binary sequence $\boldsymbol{s} = [s_1, s_2, \ldots, s_K]$ representing a message transmitted across the channel. The received bits $\boldsymbol{y} = [y_1, y_2, \ldots, y_K]$ differ from $\boldsymbol{s}$ if there is noise in the channel. Hence, the error sequence $\boldsymbol{e} = \boldsymbol{y} - \boldsymbol{s}$ describes the difference between the $\boldsymbol{y}$ and $\boldsymbol{s}$ such that $e_k = 0$ indicates the bit was received correctly while $e_k = 1$ indicates where the bit was received incorrectly.

2.1. Theoretical model for PLC and VLC

At the PLC channel, the frequency f and length l_p of the path p travelled by the signal determines the attenuation which is defined as

$$A(f, l_p) = e^{-\left(u_0 + u_1 f^{\rho}\right) l_p}. \tag{1}$$

The exponent ρ consists of values between 0.5 and 1 while u_0 and u_1 are parameters measured from the cable and they describe the initial attenuation and the frequency-related attenuation respectively. Therefore, the frequency response of the received signal is defined as

$$H(f) = \sum_{p=1}^{N} g_p \cdot A(f, l_p) \cdot e^{-j2\pi f \tau_p}, \tag{2}$$

where g_p is the path's weighting factor and $\tau_p = \frac{l_p \sqrt{\epsilon}}{c}$ describes the path's delay using the dielectric constant ϵ and speed of light c.

The occurrence of IN in the PLC channel adds to the amplitude of the transmitted signal which is simultaneously affected by background noise generated in the electronic components. Unlike background noise, IN occurs in bursts for a short period of time, hence, the probability $P(v > v_0)$ of receiving a signal whose envelope v exceeds the transmitted envelope v_0 can be defined as

$$P(v > v_0) \cong e^{-\kappa} \sum_{\mu=0}^{\infty} \frac{\kappa^{\mu}}{\mu!} e^{-\frac{v_0^2}{2\sigma_{\mu}^2}}, \quad \text{for} \quad 0 \leqslant v_0 < \infty. \tag{3}$$

where $\sigma_{\mu}^2 = \frac{\mu + \kappa\Gamma}{2\kappa(1+\Gamma)}$, Γ represents the ratio between the background noise power and IN power, κ describes the impulsive index or number of impulses per symbol duration. Since the occurrence of IN is not permanent, it can hence be modelled using the Poisson distribution [1,2,30] such that a PLC noise sample at the channel output can be defined as

$$z_{\mathrm{PLC}} = z_{\mathrm{G}} + z_{\mathrm{I}} \sqrt{D}. \tag{4}$$

The variables z_{G} and z_{I} have the respective distributions $N(0, \sigma_{\mathrm{G}}^2)$ and $N(0, \sigma_{\mathrm{I}}^2)$, implying zero mean and the variances σ_{G}^2 and σ_{I}^2 represent the Gaussian noise and IN variances respectively. The occurrence of IN is defined by the sequence D with a Poisson distribution and impulsive index κ.

Fig. 1 shows a multicarrier system which forwards a PLC signal to a VLC transmitter unit using AF. In the VLC channel, a Lambertian LED and PD follow the geometric model in Fig. 2 and the power in the transmitted signal P_{TX} is received as

$$P_{\mathrm{RX}} = hP_{\mathrm{TX}}. \tag{5}$$

Here, h is the attenuation factor of the direct line-of-sight (LOS) between the transmitter and receiver and is given as [14]

$$h = \begin{cases} \frac{A_{\mathrm{R}}(m_{\mathrm{L}}+1)}{2\pi d^2} \cos^{m_{\mathrm{L}}}(\phi_m) T_s(\psi) g(\psi) \cos\psi, & \text{for } 0 \leqslant \psi \leqslant \Psi, \\ 0, & \text{elsewhere}, \end{cases} \tag{6}$$

where $T_s(\psi)$ represents the transmitted band-pass signal, $g(\psi)$ is the gain of the imaging concentrator and m_{L} is the Lambertian factor of the source. Therefore, the received sequence for a transmitted sequence $\boldsymbol{s}$ is given as

$$\boldsymbol{y} = h\boldsymbol{s} + \boldsymbol{z}_{\mathrm{PLC}} + \boldsymbol{z}_{\mathrm{VLC}}, \tag{7}$$

where $\boldsymbol{z}_{\mathrm{PLC}}$ consists of samples defined in (4) and $\boldsymbol{z}_{\mathrm{VLC}}$ are real values with distribution $N(0, \sigma_{\mathrm{V}}^2)$ for a noise variance σ_{V}^2.

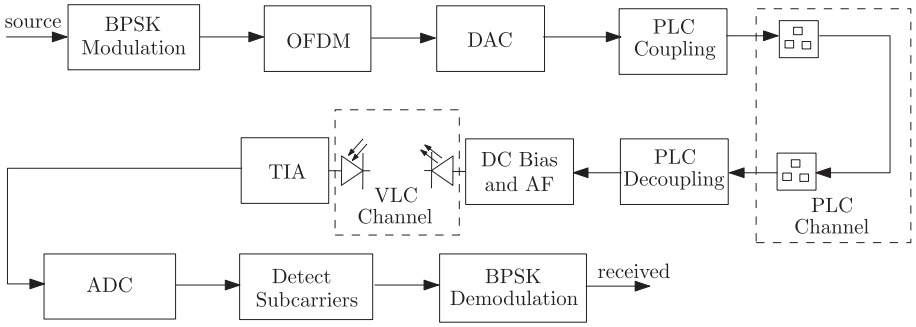

Fig. 1. Block Diagram of Hybrid AF PLC-VLC.

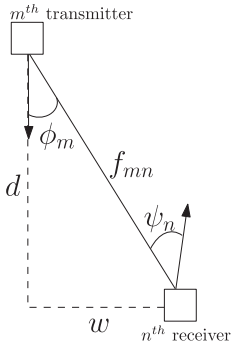

Fig. 2. Geometric model of a Lambertian LED and PD.

2.2. Markov model for memory PLC-VLC channel

For a given set of states $\boldsymbol{c} = (c_1, c_2, \ldots, c_N)$, the Markov model for the channel distribution can be defined by 3 parameters $X = [A, B, \Pi]$. The transition probability matrix $A(t) = [a_{ij}(t)]$ represents the probability of the channel transitioning into a different state or remaining in the same state between observation period t and t_{n+1}. Each element a_{ij} represents the probability of transitioning from state i to state j.

The present state of the model at t is described by a set of probabilities $\Pi_t = [\pi_{t,1}, \pi_{t,2}, \ldots, \pi_{t,n}]$. Using the transition probability matrix $A(t)$, the state probability distribution at $t+1$ is

$$\Pi_{t+1} = \Pi_{t+1} A. \tag{8}$$

The aim is to iterate Π until it attains a steady state probability distribution Π_{ss} at iteration k. Therefore, if

$$\begin{aligned} \Pi_{t+k} &= \Pi_{t+k} A, \\ &= \Pi_t A^k, \end{aligned} \tag{9}$$

then

$$\Pi_{ss} = \Pi_{ss} A^k, \tag{10}$$

at the k-th iteration.

The error state probability matrix $B = [b_{ij}]$ describes the probabilities of the model making a correct or incorrect decision given its current state. Hence,

$$\sum_{n=1}^{N} b_i = 1, \qquad \sum_{n=1}^{N} b_j = 1. \tag{11}$$

2.3. Fritchman model

The Fritchman model suits channels with burst errors such as the PLC channel by grouping the channel states into two groups of k good states and $N-k$ bad states [25] as shown in Fig. 3. Assuming the absence of external interference such as external illumination, the noise model of the VLC channel is predominantly Gaussian. Hence, a 3-state model as shown in Fig. 3 is chosen to model the PLC-VLC channel such that the transition probability of the channel remaining in a good state is higher than the probability of transitioning to a bad state while in a good state. Two states represent the good states while one state represents the bad state. Therefore, the state transition probabilities are

$$A = \begin{bmatrix} a_{11} & 0 & a_{13} \\ 0 & a_{22} & a_{23} \\ a_{31} & a_{32} & a_{33} \end{bmatrix}. \tag{12}$$

The error state probability B is therefore

$$B = \begin{bmatrix} 1 & 1 & 0 \\ 0 & 0 & 1 \end{bmatrix}. \tag{13}$$

2.4. Baum-Welch algorithm

In order to find the maximum likelihood parameters $X = \{A, B\}$ that maximize $\Pr(\bar{O}|X)$, the Baum-Welch algorithm [28] iterates until it converges into an estimated $X = \left\{\widehat{A}, \hat{B}\right\}$. The estimated elements of $\widehat{A}$ are defined as

$$\begin{aligned} \hat{a}_{ij} &= \frac{\text{expected number of transitions from } i \text{ to } j}{\text{expected number of transitions from } i}, \\ &= \frac{\sum_{t=1}^{T-1} \xi_t(i,j)}{\sum_{t=1}^{T-1} \gamma_t(i)}, \end{aligned} \tag{14}$$

while the estimated elements of $\hat{B}$ are defined as

$$\begin{aligned} \hat{b}_j(e_k) &= \frac{\text{expected number of times } e_k \text{ is emitted from state } j}{\text{expected number of visits to state } j}, \\ &= \frac{\sum_{t=1|O_t=e_k}^{T} \gamma_t(j)}{\sum_{t=1}^{T} \gamma_t(j)}. \end{aligned} \tag{15}$$

The term

$$\begin{aligned} \xi_t(i,j) &= \Pr\left[s_t = i, s_{t+1} = j | \bar{O}, X\right], \\ &= \frac{\alpha_t(i) a_{ij} b_j\left(O_{t+1}\right) \beta_{t+1}(j)}{\Pr\left[\bar{O}|X\right]}, \end{aligned} \tag{16}$$

and

$$\begin{aligned} \gamma_t(i) &= \Pr\left[s_t = i | \bar{O}, X\right], \\ &= \frac{\alpha_t(i)\beta_t(i)}{\Pr\left[\bar{O}|X\right]} \quad i = 1, 2, \ldots, N. \end{aligned} \tag{17}$$

From Eq. (16) and (17), the forward variables $\alpha_t(i)$ are determined by initializing at $t = 1$

$$\alpha_1(i) = \pi_i b_i(O_1), \quad i = 1, 2, \ldots, N, \tag{18}$$

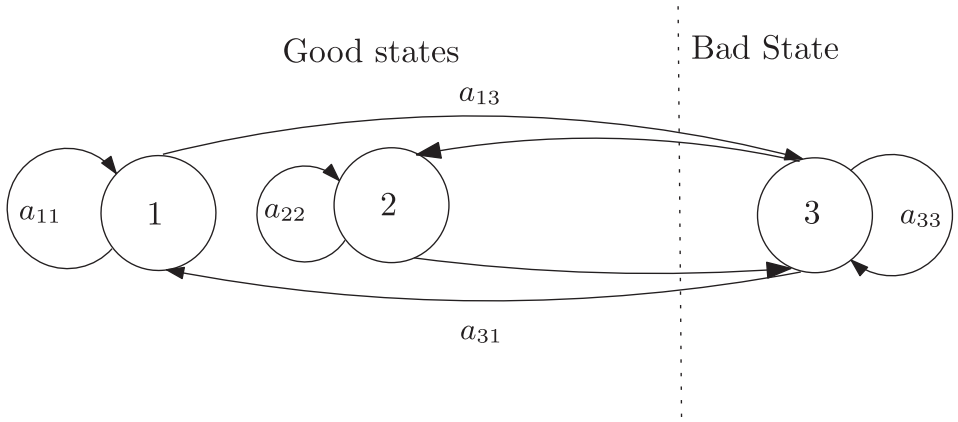

Fig. 3. Fritchman Model with 3 States.

then at $t > 1$,

$$\alpha_{t+1}(i) = \left[\sum_{i=1}^{N} \alpha_t(i) a_{ij}\right] b_i(O_{t+1}), \quad \text{for } 1 \leqslant t \leqslant T-1,\ 1 \leqslant j \leqslant N, \tag{19}$$

and terminated at condition

$$Pr\left[\bar{O}|X\right] = \sum_{i=1}^{N} \alpha_T(i)\beta_T(i), \tag{20}$$

where

$$\sum_{i=1}^{N} \alpha_T(i) = \sum_{i=1}^{N} Pr[O_1, \ldots, O_T, s_T = i|X] = Pr\left[\bar{O}|X\right]. \tag{21}$$

At $t = 1$, the backward variables $\beta_t(i)$ are initialized for all N states

$$\beta_1(i) = 1, \quad i = 1, 2, \ldots, N, \tag{22}$$

and at $t > 1$,

$$\beta_t(i) = \sum_{i=1}^{N} \beta_{t+1}(j) b_j(O_{t+1}) a_{ij}, \quad \text{for } 1 \leqslant t \leqslant T-1,\ 1 \leqslant j \leqslant N. \tag{23}$$

2.5. Semi-Hidden Fritchman HMM

Error sequences are generated from each frame transmitted as a vector of binary bits over the channel. For simplicity, a randomly composed text message of 70 letters including spaces, which translate to 560 bits are used. The frames are repeatedly transmitted 100 times in order to generate 5.6×10^4 bits. An error sequence vector is then generated to represent the Hamming distance between the sent vector and received vector. Where the index of the sent and received bits are the same, a "0" is stored in the error sequence vector. Otherwise, a "1" is stored in the error sequence vector. We initialize $X = \{A, B, \Pi\}$ as follows

$$A = \begin{bmatrix} 0.68 & 0 & 0.32 \\ 0 & 0.79 & 0.21 \\ 0.48 & 0.45 & 0.07 \end{bmatrix},$$

$$B = \begin{bmatrix} 1 & 1 & 0 \\ 0 & 0 & 1 \end{bmatrix},$$

and

$$\Pi = [0.47 \quad 0.47 \quad 0.06].$$

3. Experimental setup and measurements

Fig. 1 shows a block diagram of the experimental setup of the hybrid system. Multi-carrier OFDM with BPSK is used to transmit the incoming information over an indoor PLC link. The OFDM-BPSK signals are designed using MATLAB and converted to analogue signals for transmission over a USRP N210 software-defined radio. The USRP transmitter (Tx) converts the modulated OFDM signal to analogue samples in order to transmit over the PLC channel. The narrowband PLC coupling unit provides galvanic isolation and filtering. At the output of the PLC channel, the PLC signal is amplified with an amplification factor A_V and a direct current (DC) bias is added to the amplified signal. The PLC signal hence modulates the intensity of the LED which is always ON as a result of the DC voltage.

The error sequence measurements are obtained in an indoor office environment using the testbed in Fig. 4(a) with the transmitter and receiver units of the VLC shown in Fig. 4(b) and (c) respectively. The parameters for the USRP radio and transmitted message are also defined in Table 1. These measurements are then used as training data to derive the steady-state transition probabilities of the channel using the Baum-Welch algorithm [28] and the initialized FM parameters $X = \{A, B, \Pi\}$ as input. The resulting transition probabilities are then used to re-generate and obtain an approximate, statistical error sequence using the error vector generation algorithm [29] in order to validate the accuracy of the resulting channel models. An isolation transformer is used to block the impulse that may be injected into the power-line from devices plugged into the power-line bus network in the office. Measurements are taken in a 0 Watt (W) scenario, where other than the coupling circuits, no devices are connected to the power-line. Measurements are also taken in a 11 W scenario where a table lamp with an 11 W bulb is plugged into the power-line channel in order to create impulse disturbance from a constant voltage source. In order to have negligible attenuation due to distance in the PLC link, a considerably short PLC link length of approximately 2 meters is used.

For the VLC link, the geometric model in Fig. 2 is used and measurements are taken for different values of w. The AF unit of the VLC transmitter in Fig. 5a uses an operational amplifier to amplify the PLC signal with a gain $A_V = 1.45$ using a DC voltage $V_1 = 1.45$ Volts. The off-the-shelf A3 series white LEDs used at the transmitter are not suitable for high frequency signals as they do not switch fast enough, hence the choice of 200 kHz center frequency in the USRP.

The VLC receiver in Fig. 5b consists of an SFH 213 PD with a TIA unit which converts the intensity captured by the PD to an equivalent current. This current is converted to its equivalent voltage V_{TIA} and passed on to the USRP receiver (Rx). The receiver then

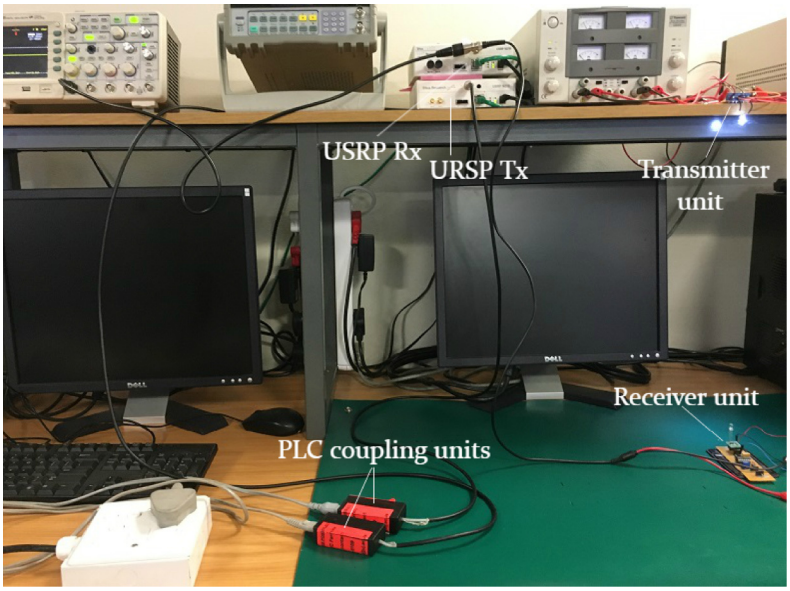

(a) Hybrid AF PLC-VLC indoor laboratory testbed

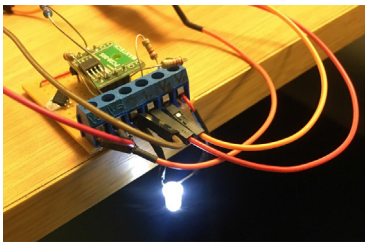

(b) VLC transmitter unit

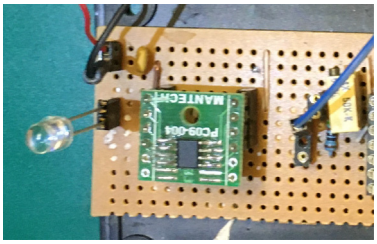

(c) VLC receiver unit

Fig. 4. Testbed showing USRP radios with PLC link to VLC AF transmitter and VLC receiver.

Table 1
USRP and modulation parameters.

Parameter	Value
Center frequency	200 kHz
Sampling frequency	1 MHz
FFT Length	64
Message Length	560 bits per frame

samples the received voltages such that the received samples are demodulated to recover the likely transmitted bits.

4. Results

4.1. Estimated model (state transition probabilities)

Table 2 shows the first order estimated model parameters (estimated state transition probabilities) at steady state given the measured error sequence for the different values of w in centimeters (cm), with and without the 11 W load connected to the power line.

The estimated state transition probabilities show the model parameters that characterize the measured error sequences from an indoor PLC-VLC channel. It can be deduced from Table 2 that there are non-uniform estimated state transition probability values. This non-uniformity in estimated state transition probability distribution is attributed to the non-identical bit error sequences measured as a result of the different scenarios where w (cm) is varied with and without a load connected.

4.2. Estimated model validation

The aim of any channel modeling is to obtain the most probable parameter set given a measured or simulated dataset. Hence, it is important to analytically validate the fitness and accuracy of the estimated model derived in Section 4.1. The log-likelihood ratio (LLR), the error-free run distribution (EFRD) and the error probabilities are used to validate a close match between the measured and model generated error sequences in Sections 4.2.1, 4.2.2, 4.2.3 respectively thus ascertaining the accuracy of the derived models.

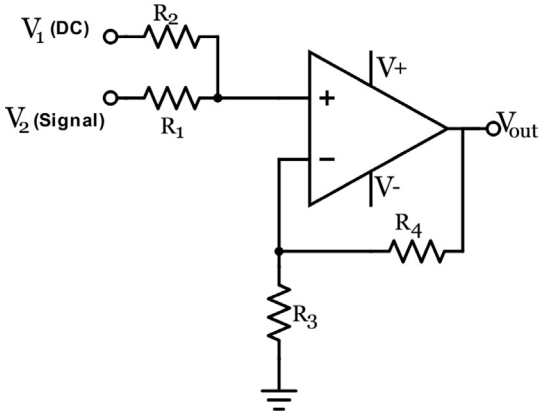

(a) AF unit that supplies DC bias voltage to signal voltage.

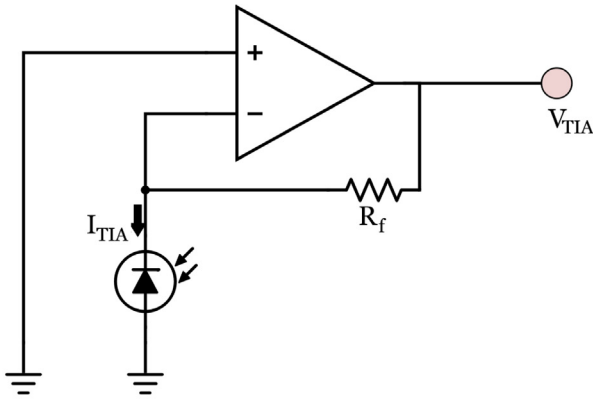

(b) Receiver unit that uses a TIA to convert transmitted current to voltage.

Fig. 5. AF LED transmitter and receiver using TIA and PD.

Table 2
Estimated Models (estimated state transition probabilities).

w (cm)	Load (W)	a_{11}	a_{13}	a_{22}	a_{23}	a_{31}	a_{32}	a_{33}
0	0	0.8952	0.1048	1.0000	0.0000	0.4647	0.0026	0.5326
	11	0.7007	0.2993	0.9989	0.0011	0.3993	0.0611	0.5396
1	0	0.8965	0.1035	1.0000	0.0000	0.4852	0.0032	0.5116
	11	0.5895	0.4105	0.9990	0.0010	0.4687	0.0425	0.4888
2	0	0.7070	0.2930	1.0000	0.0000	0.6291	0.0013	0.3696
	11	0.7324	0.2676	0.9994	0.0006	0.4482	0.0590	0.4928
3	0	0.6790	0.3210	1.0000	0.0000	0.5583	0.0013	0.4404
	11	0.7852	0.2148	0.9995	0.0005	0.4474	0.0465	0.5062
4	0	0.4898	0.5102	1.0000	0.0000	0.5020	0.0026	0.4954
	11	0.6158	0.3842	0.9993	0.0007	0.4842	0.0452	0.4706
5	0	0.6641	0.3359	1.0000	0.0000	0.5628	0.0014	0.4358
	11	0.7141	0.2859	0.9994	0.0006	0.4379	0.0387	0.5234
6	0	0.5518	0.4482	1.0000	0.0000	0.4916	0.0008	0.5076
	11	0.5514	0.4486	0.9993	0.0007	0.4730	0.0226	0.5043
7	0	0.8962	0.1038	1.0000	0.0000	0.4476	0.0025	0.5499
	11	0.6947	0.3053	0.9991	0.0009	0.3254	0.0538	0.6207
8	0	0.7078	0.2922	0.9998	0.0002	0.5462	0.0143	0.4395
	11	0.5405	0.4595	0.9715	0.0285	0.4501	0.0542	0.4957
9	0	0.6114	0.3886	0.9978	0.0022	0.4983	0.0216	0.4801
	11	0.4715	0.5285	0.9323	0.0677	0.3984	0.1032	0.4984
10	0	0.5038	0.4962	0.8505	0.1495	0.4244	0.1203	0.4553
	11	0.4879	0.5121	0.9264	0.0736	0.4007	0.0987	0.5006

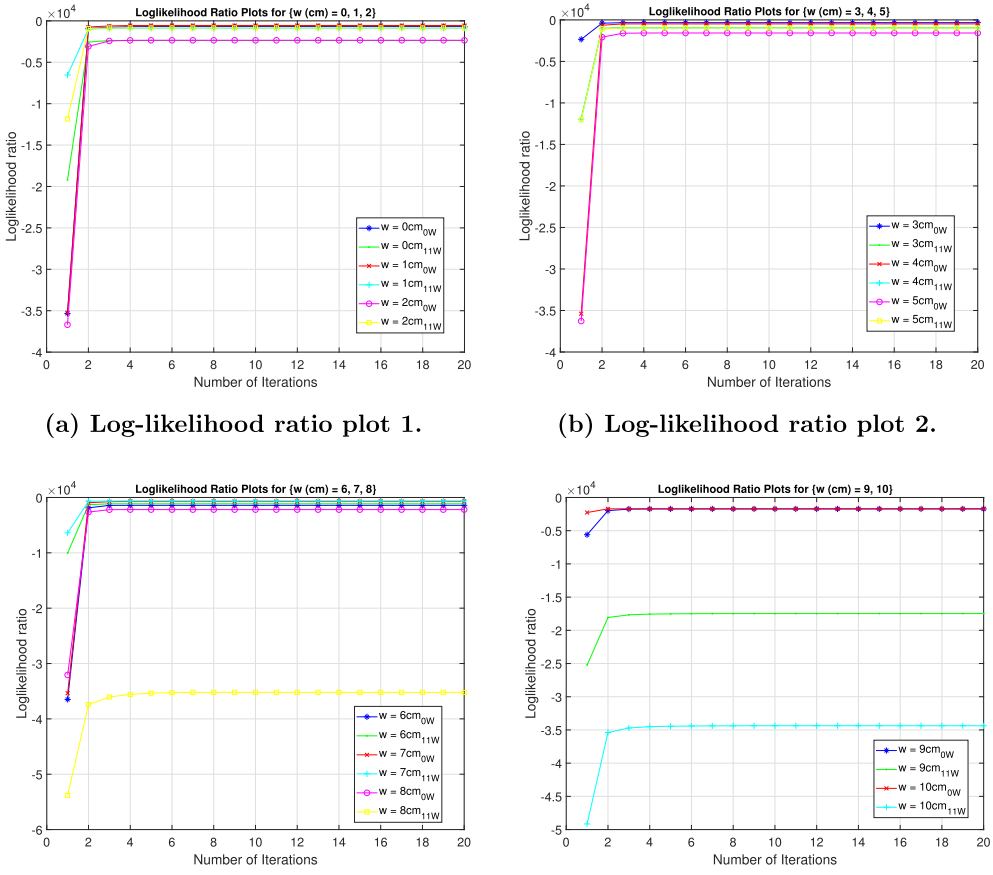

(a) Log-likelihood ratio plot 1.

(b) Log-likelihood ratio plot 2.

(c) Log-likelihood ratio plot 3.

(d) Log-likelihood ratio plot 4.

Fig. 6. Log-likelihood ratio plots.

4.2.1. Log-likelihood ratio plots

In order to obtain a derived model that closely matches the measured data, the LLR assists with obtaining a set of model parameters that maximize the likelihood function. For a mathematical representation and description of the LLR, refer to [31].

Fig. 6a, b, c and d show the LLR plot for models realized for the different values of *w*, with and without the 11 W load connected. It can be deduced from these Figures that the model starts to converge at the second iteration with a negative LLR value relatively close to zero validating the model accuracy. The LLR plot alone can-

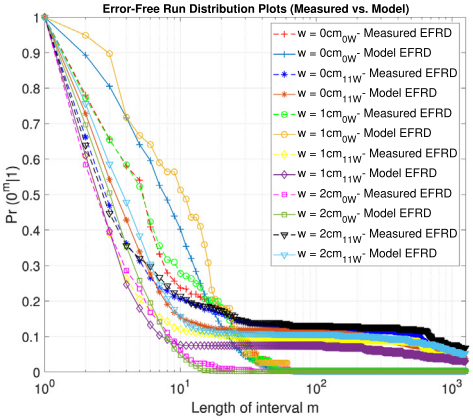

(a) Measured vs. model-generated EFRD 1.

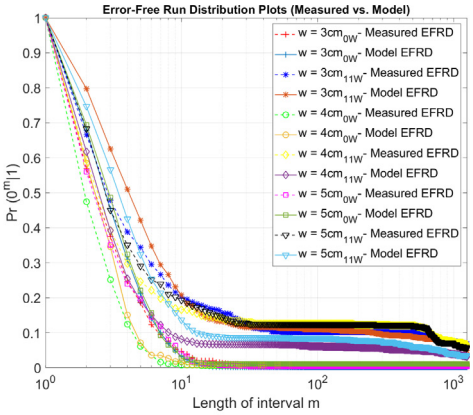

(b) Measured vs. model-generated EFRD 2.

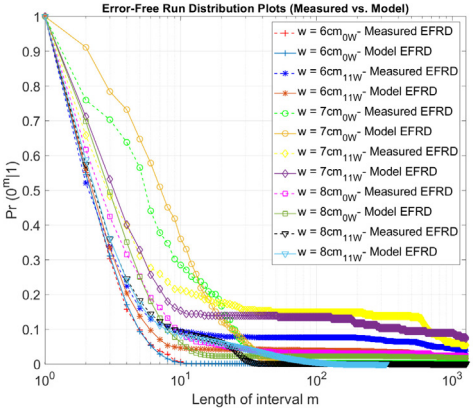

(c) Measured vs. model-generated EFRD 3.

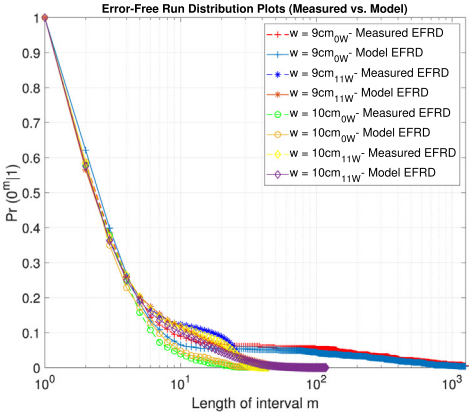

(d) Measured vs. model-generated EFRD 4.

Fig. 7. Measured vs. model-generated EFRD.

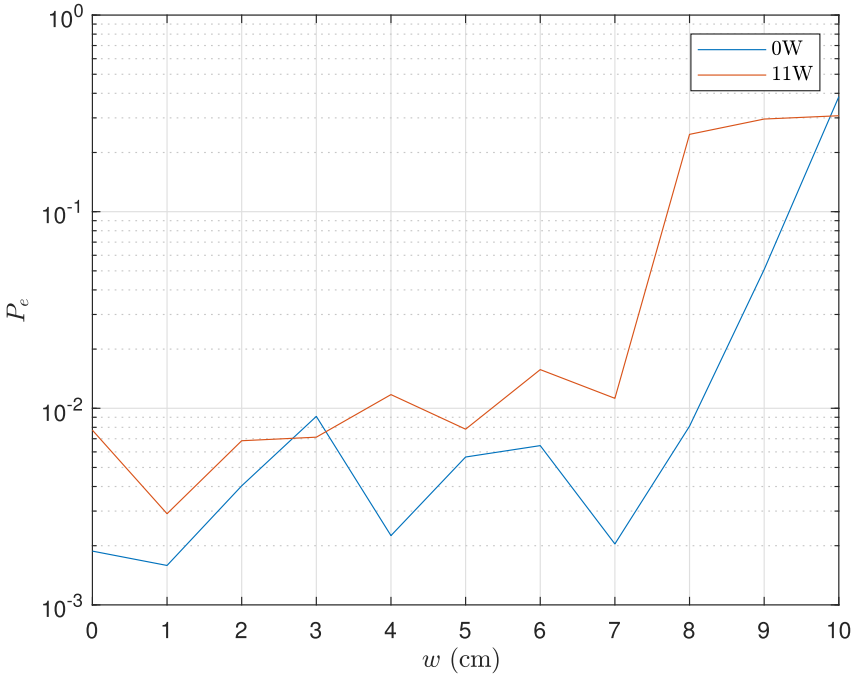

Fig. 8. Probability of error for different values of w with $d = 40$ cm measured from the hybrid channel.

Table 3
Error probabilities comparison ((P_e) - measured sequence vs. $(\bar{P}_e)$ - model regenerated sequence.

w (cm)	Load (W)	P_e	$\bar{P}_e$
0	0	0.0019	0.0027
	11	0.0135	0.0143
1	0	0.0016	0.0017
	11	0.0029	0.0025
2	0	0.0059	0.0066
	11	0.0068	0.0077
3	0	0.0091	0.0084
	11	0.0071	0.0079
4	0	0.0023	0.0029
	11	0.0117	0.0125
5	0	0.0057	0.0053
	11	0.0078	0.0087
6	0	0.0065	0.0064
	11	0.0157	0.0166
7	0	0.0020	0.0025
	11	0.0112	0.0120
8	0	0.0081	0.0086
	11	0.2473	0.2458
9	0	0.0508	0.0513
	11	0.2959	0.3085
10	0	0.3843	0.3827
	11	0.3076	0.3167

not be employed to measure the accuracy of a model as these values are a function of data size and can otherwise be applied in determining the most accurate of different model parameters obtained from the same error sequence.

4.2.2. Error-free run distribution plots

The EFRD denoted by $Pr(0^m|1)$ implies the probability of transitioning from an error state to m consecutive error-free states. The EFRD probabilities are obtained for the measured error sequences. Using the estimated model parameter for each measured error sequence obtained, we generated an error sequence of the same length as the measured error sequence and then obtain the EFRD probabilities for these model generated error sequences. A comparison between measured EFRD and model EFRD is then carried out to validate the accuracy of the derived models.

Fig. 7a, b, c and d show a comparison of the measured EFRD and model EFRD for models realized for the different vaues of w, with and without the 11 W load connected. It can be deduced from Fig. 7a, b, c and d that a close match exist between the measured EFRD and model EFRD validating the accuracy of the derived models. It can also be seen in Fig. 7a, b, c and d respectively that $Pr(0^m|1)$ denoting the EFRD is a monotonically decreasing function of m, that is $Pr\left(0^0|1\right) = 1$ and similarly $Pr(0^m|1) \rightarrow 0$ as the length of interval denoted by m increases.

4.2.3. Error probabilities

Fig. 8 shows the bit error rate (BER) from the measured sequences for different values of w. As the value of w increases, the number of errors increase due to the attenuation h on the signal power. The effect of the noise introduced into the PLC link by the 11 W load also becomes evident in the poorer BER performance for most values of w when compared with the 0 W scenario. As w increases, the noise power dominates the signal power, hence more errors as shown in Fig. 8.

The error probabilities of the measured and the model generated error sequences are obtained in order to validate the accuracy of the derived models. A close match between the error probabilities of the measured and model generated error sequences validate the accuracy of the derived models. Table 3 shows the error probabilities for the measured and model generated error sequences for the different values of w, with and without the 11 W load. It can be deduced from Table 3 that a close match exist between the error probabilities of the measured and model generated error sequences thus validating the accuracy of the derived models for the indoor PLC-VLC channel.

5. Conclusion

The error distribution of an indoor, hybrid AF PLC-VLC channel with memory is evaluated by taking error sequence measurements from the testbed with the aid of OFDM-BPSK modulation with USRP N210 radios. EFR distributions are determined from the measured error sequences in order to characterize the error distribution using the measurements from different channel conditions, under different channel disturbances. The Baum-Welch re-estimation algorithm is then used to develop statistical model parameters for the corresponding channel conditions and disturbances. The measured and re-estimated model parameters show close matches based on the chosen initial and derived parameters for the different channel conditions. The closeness of the $\bar{P}_e$ of the error sequence generated from the estimated model with the measured P_e indicate the suitability of the SHMM and the derived statistical model parameters. For future work, signal models, modulation and coding techniques suitable for reducing the $\bar{P}_e$, especially in conditions corresponding to higher $\bar{P}_e$ can be further investigated.

Declaration of Competing Interest

The authors declare that they have no known competing financial interests or personal relationships that could have appeared to influence the work reported in this paper.

Acknowledgement

The authors would like to thank and acknowledge the financial support provided by the Optical Communication Laboratory (OCL) and the Sibanye-Stillwater Digital Mining Laboratory (DigiMine), Wits Mining Institute (WMI), University of the Witwatersrand, Johannesburg, South Africa.

Appendix A. Supplementary material

Supplementary data associated with this article can be found, in the online version, at https://doi.org/10.1016/j.aeue.2020.153108.

References

[1] Middleton D. Statistical-physical model of electromagnetic interference. IEEE Trans Electromagn Compatib 1977;3:106–27.
[2] Middleton D. Non-Gaussian noise models in signal processing for telecommunications: new methods an results for class a and class b noise models. IEEE Trans Inf Theory 1999;45(4):1129–49.
[3] Middleton D. Canonical and quasi-canonical probability models of class a interference. IEEE Trans Electromagn Compatib 1983;EMC-25(2):76–106.
[4] Zimmermann KDM. A multipath model for the powerline channel. IEEE Trans Commun 2002;50(4):553–9.
[5] Hooijen OG. On the channel capacity of the residential power circuit used as a digital communications medium. IEEE Commun Lett 1998;2(10):267–8.
[6] Song J, Liu S, Zhou G, Yu B, Ding W, Yang F. et al. A cost-effective approach for ubiquitous broadband access based on hybrid plc-vlc system. In: 2016 IEEE international symposium on circuits and systems (ISCAS); 2016. p. 2815-8.
[7] Ding W, Yang F, Yang H, Wang J, Wang X, Zhang X, et al. A hybrid power line and visible light communication system for indoor hospital applications. Comput Ind 2015;68:170–8.
[8] Ma LLH, Hranilovic S. Subcarrier allocation in hybrid visible light and power line communication system. In: 2016 IEEE international symposium on circuits and systems (ISCAS); 2016. p. 2819-22.
[9] Komine T, Haruyama S, Nakagawa M. Performance evaluation of narrowband OFDM on integrated system of power line communication and visible light wireless communication. In: 2006 1st international symposium on wireless pervasive computing; 2006. p. 6.

[10] Ndjiongue AR, Shongwe T, Ferreira HC, Ngatched TMN, Vinck AJH. Cascaded plc-vlc channel using ofdm and csk techniques. In: 2015 IEEE global communications conference (GLOBECOM); 2015. p. 1-6.
[11] Komine T, Nakagawa M. Integrated system of white LED visible-light communication and power-line communication. In: The 13th IEEE international symposium on personal, indoor and mobile radio communications, vol. 4; 2002. p. 1762–6.
[12] Ma X, Gao J, Yang F, Ding W, Yang H, Song J. Integrated power line and visible light communication system compatible with multi-service transmission. IET Commun 2017;11(v1):104–11.
[13] Kolade O, Cox M, Cheng L. Visible light communication using a software-defined radio approach. In: Fifth conference on sensors, MEMS, and electro-optic systems:11043. https://doi.org/10.1117/12.2502064.
[14] Gfeller FR, Bapst U. Wireless in-house data communication via diffuse infrared radiation. Proc IEEE 1979;67(11):1474–86.
[15] Nlom SM, Ndjiongue AR, Ouahada K, Ferreira HC, Vinck AJH, Shongwe T. A simplistic channel model for cascaded plc-vlc systems. In: 2017 IEEE international symposium on power line communications and its applications (ISPLC); 2017. p. 1–6.
[16] Ndjiongue AR, Ferreira HC, Song J, Yang F, Cheng L. Hybrid PLC-VLC channel model and spectral estimation using a nonparametric approach. Trans Emerg Telecommun Technol 28(12):e3224. https://onlinelibrary.wiley.com/doi/abs/10.1002/ett.3224.
[17] Howard RA. Dynamic probabilistic systems: Markov models:1. Courier Corporation; 2012.
[18] Rabiner LR, Juang B-H. An introduction to hidden Markov models. ieee assp magazine 3–1: 4–16.
[19] Wang HS, Moayeri N. Finite-state Markov channel-a useful model for radio communication channels. IEEE Trans Veh Technol 1995;44(1):163–71.
[20] Gilbert EN. Capacity of a burst-noise channel. Bell Syst Tech J 1960;39(5):1253–65.
[21] Sivaprakasam S, Shanmugan KS. An equivalent Markov model for burst errors in digital channels. IEEE Trans Commun 43–2/3/4:1347–55.
[22] Familua AD. A block diagonal Markov model for indoor software-defined power line communication. In: 2019 IEEE PES/IAS PowerAfrica, Abuja, Nigeria; 2019. p. 1-6.
[23] Ndo FLG, Kassouf M. A Markov-Middleton model for bursty impulsive noise: Modeling and receiver design. IEEE Trans Power Deliv 2013;28(4):2317–25.
[24] Familua AD, Cheng L. First and second-order semi-hidden Fritchman Markov models for a multi-carrier based indoor narrowband power line communication system. Phys Commun 2018;29:55–66. http://www.sciencedirect.com/science/article/pii/S1874490717302343.
[25] Fritchman B. A binary channel characterization using partitioned Markov chains. IEEE Trans Inform Theory 1967;13(2):221–7.
[26] Holmes G, Cheng L, Shimaponda-Nawa M, Familua AD, Abu-Mahfouz AM. Modelling noise and pulse width modulation interference in indoor visible light communication channels. AEU - Int J Electron Commun 2019;106:40–7. http://www.sciencedirect.com/science/article/pii/S1434841119301451.
[27] Familua AD, Ndjiongue AR, Ogunyanda K, Cheng L, Ferreira HC, Swart TG. A semi-hidden Markov modeling of a low complexity FSK-OOK in-house PLC and VLC integration. In: 2015 IEEE international symposium on power line communications and its applications (ISPLC); 2015. p. 199–204.
[28] Baum LE, Petrie T, Soules G, Weiss N. A maximization technique occurring in the statistical analysis of probabilistic functions of Markov chains. Ann Math Stat 1970;41(1):164–71.
[29] Tranter W, Shanmugan K, Rappaport T, Kosbar K. Principles of communication systems simulation with wireless applications, 1st ed. . Prentice Hall Press; 2003. p. 601–23 [chapter 15].
[30] Andreadou N, Pavlidou F. PLC, channel: Impulsive noise modelling and its performance evaluation under different array coding schemes. IEEE Trans Power Deliv 2009;24(2):585–95.
[31] Familua AD, Cheng L. A semi-hidden Fritchman Markov modeling of indoor CENELEC A narrowband power line noise based on signal level measurements. AEU-Int J Electron Commun 2017;74:21–30.

Oluwafemi Kolade is currently studying for his PhD degree in Telecommunications at the University of the Witwatersrand (Wits), South Africa. Prior to this, he obtained a bachelor's degree in 2010 in Electronics and Electrical Engineering at the Obafemi Awolowo University, Ile-Ife, Nigeria. He then completed his MSc in Electrical and Information Engineering at Wits in 2017. His research focuses on signal processing, error correction, power line and optical communications. He is also a member of the Digital Mining laboratory at Wits where he applies his telecommunications experience to the underground mining environment. Between 2010 and 2015, he worked in industry where he co-founded and led software development teams at Exolve Technologies, Lagos before returning to academia in 2015 for his MSc degree.

Ayokunle Damilola Familua received his B-Eng Electrical and Electronics Engineering from the Federal University of Technology Akure in 2007, MSc degree in Electrical Engineering in 2013 and PhD in Electrical Engineering in 2017 from the University of the Witwatersrand, Johannesburg, South Africa. He is currently a Postdoctoral Research Fellow with Center for Telecommunications, Department of Electrical and Electronic Engineering Science, University of Johannesburg, South Africa and an associate member of the optical communication labs - WITS University. His research interests are in developing Digital Communications and Networks for Intelligent Systems in the Fourth Industrial Revolution with specific focus on the Internet of Things (IoT), Power Line Communication, Visible Light Communication, and other wired and wireless communication technologies. He also has special interest in channel modeling using Ma chine Learning algorithms and Artificial Intelligence. He has published 15 journals and conference proceedings. Ayokunle is a recipient of the best student paper award at the IEEE ISPLC 2015 conference held in Austin Texas, United States. He is also a recipient of the following awards: Top Outstanding Performer, Top Achiever for Core Network and Wireless Packet Switching Fundamentals in the 2014 Huawei Technologies South Africa Graduate training programme. He is a Huawei Certified Network Associate - Routing Switching (HCNA R & S).

Ling Cheng received the degree B. Eng. Electronics and Information (cum laude) from Huazhong University of Science and Technology (HUST) in 1995, M. Ing. Electrical and Electronics (cum laude) in 2005, and D. Ing. Electrical and Electronics in 2011 from University of Johannesburg (UJ). His research interests are in Telecommunications and Artificial Intelligence. In 2010, he joined University of the Witwatersrand where he was promoted to Full Professor in 2019. He has served as the Vice-chair of IEEE South African Information Theory Chapter. He has been a visiting professor at four universities and the principal advisor for over forty full research post-graduate students. He has published more than 90 research papers in journals and conference proceedings. He was awarded the Chancellor's medals in 2005, 2019 and the National Research Foundation rating in 2014. The IEEE ISPLC 2015 best student paper award was made to his Ph.D. student in Austin.